New Journal of Glass and Ceramics, **2011, 1, 1-19**
Published Online April 2011 in SciRes (http://www.SciRP.org/journal/njgc/)

TABLE OF CONTENTS

Volume 1 Number 1 April 2011

New Journal of Glass and Ceramics (NJGC)

Journal Information

SUBSCRIPTIONS

The *New Journal of Glass and Ceramics* (Online at Scientific Research Publishing, www.SciRP.org) is published quarterly by Scientific Research Publishing, Inc., USA.

Subscription rates:

Print: $39 per issue.
To subscribe, please contact Journals Subscriptions Department, E-mail: sub@scirp.org

SERVICES

Advertisements
Advertisement Sales Department, E-mail: service@scirp.org

Reprints (minimum quantity 100 copies)
Reprints Co-ordinator, Scientific Research Publishing, Inc., USA.
E-mail: sub@scirp.org

COPYRIGHT

PRODUCTION INFORMATION

For manuscripts that have been accepted for publication, please contact:
E-mail: njgc@scirp.org

New Journal of Glass and Ceramics, **2011, 1, 1-6**
doi:10.4236/njgc.2011.11001 Published Online April 2011 (http://www.SciRP.org/journal/njgc)

Scientific Research

The Effect of Using Nano ZrO_2 on the Properties of W-ZrC Composite Fabricated through Reaction Sintering

Mostafa Roosta[1], Hamidreza Baharvandi[1], Hossein Abdizade[2]

[1]Malek Ashtar University of Technology, Tehran, Iran;
[2]School of Metallurgy and Materials Engineering, University of Tehran, Tehran, Iran.
Email: mostafa_rosta@yahoo.com

Received January 10th, revised March 21st, 2011; accepted April 9th, 2011.

ABSTRACT

To fabricate W-ZrC composite through reaction sintering at first WC and ZrO_2 powders with molar ratio of 3-1 *are ball milled, then the green body made from this mixture is sintered. Since reactivity is the main problem in sintering of micronized powders the starting ZrO_2 powder is selected in nano size to see whether the reaction improves. The XRD pattern indicates that W-ZrC composite has been formed, although some unreacted compounds still exist and some unwanted components have been created. In the case of using nano powders the amount of unreacted WC and ZrO_2 phases and unwanted W_2C phase reduces and the reaction progresses better. Additionally by using nano powders the reaction progressed and the mechanical proprieties including density, hardness, Elastic modulus and Flexural strength improved.*

Keywords: *W/ZrC Composite*, *Reaction Sintering*, *Tungsten Carbide*, *Nano Zirconium Oxide*

1. Introduction

To improve low-temperature plasticity in tungsten and its strength at high temperature, making composite is an effective way. W-Cu and W-ZrC are the examples of such composites. Strength at high temperature and thermal shock resistance of those composites caused their application at high temperature environments, such as the nozzle throat of solid fuel rocket. In fact the ZrC has low coefficient of thermal expansion, high elastic modulus, good strength at high temperatures and low thermal conductivity. Also it is compatible with tungsten because they have a comparable melting point, similar coefficient of linear expansion and both have relatively high thermal conductivity. Furthermore W and ZrC exhibit little mutual solid solubility at high temperature and do not react to form other compounds. The density of zirconium carbide is almost one third of tungsten which results in a lighter composite. Consequently W and ZrC make a preferable composite [1-3].

Three way of production has been reported for fabrication of W/ZrC composites:

1) Displacive compensation of porosity (DCP): Porous WC preforms are produced by gel casting, hot isostatic pressing or other conventional ceramic processes and then the porous preform will be exposed to molten Zr_2Cu at 1200 - 1300˚C and ambient pressure. The Zr_2Cu liquid rapidly infiltrate into the preform and undergoes a displacement reaction with WC to yield dense ZrC/W composite. Among the advantages of this process are less required pressure and heat rather than hot press, possibility of making larger and more complex parts and lower cost, but being a two-stage method, retention of copper-rich phase which usually makes unwanted impurities with a low melting temperature within the composite and inability to control the exact size and porosity of the preform and therefore production of the same part are the disadvantages of this method [1-4].

2) Hot-press: This method is one of the most expensive and perhaps the most common processes used for making composites because of its simplicity. It is similar to warm sintering unless the temperature and pressure are applied simultaneously. Of all advantages that this method contains, increasing the properties of row and sintered material such as density, strength and fatigue properties is the main one. Other advantages of this method are less grain growth, less porosity, higher strength and improving the high temperature properties. However simple

shape of made parts which needs further machining decreases the speed of the production and increases the cost. High pressure and high temperature required in this method are the main disadvantage of hot pressing [5-12].

3) Reaction sintering: It is a new method for producing W/ZrC composite in which metal powders are subjected to high temperatures, typically in an inert atmosphere or under vacuum. In this method ZrO_2 and WC powders are mixed in desired volume or mass fraction, at the presence of a suitable binder. The mixed powders then form a green body which at the next stage is heated at a temperature sufficient for the binder to be volatilized, between 400 - 600˚C and then the temperature is elevated up to 1850˚C to produce an oxide-reduced or partially-sintered body. The temperature of the partially sintered body is then raised to 2100˚C to complete the densification [13].

In this study, the W-ZrC composite is fabricated by reaction sintering of WC and ZrO_2 Powders that are selected in micron and nano size to see the differences between the resultant composites. One objective of the present study is to investigate the changes after using the nano particles instead of micron particles. Therefore in order to compare the composites at first a sample reference is made from micron powders, then it will be compared with a composite that has been made by using nano powders. For this the volume fraction of different phases which has been formed in both composites is approximately estimated by the ratio of the integrated area of the peaks and the total XRD patterns [14] to see the efficiency of process. The densities of best obtained samples are determined using Archimedes method, according to ASTM B311 standard method. The hardness is evaluated in accordance with ASTM E10. Moreover the bending strength of the composite has been measured by bending test according to ASTM C1161 and the modulus of elasticity is measured as well, by ASTM C1419 test standard method. Also by secondary electron microscopy (SEM) and back scattered electron (BSE) the morphology of samples are studied.

2. Experimental

Commercial tungsten carbide powder (d_{50} = 2 μm, purity = 99.5%) and zirconium oxide (in two sizes d_{50} = 75 nm and d_{50} = 1 μm, purity = 99.6%) are used as raw materials. **Figure 1** shows the morphology and particle size of these starting powders.

To fabricate W/ZrC composite through reaction sintering method, at first ZrO_2 and WC powder were mixed at presence of a binder so that a precursor was formed. To produce a workpiece weighing 150 g, WC and ZrO_2 powders are mixed according to **Table 1** with optimum molar ratio of 3 - 1 [13] between WC and ZrO_2, although

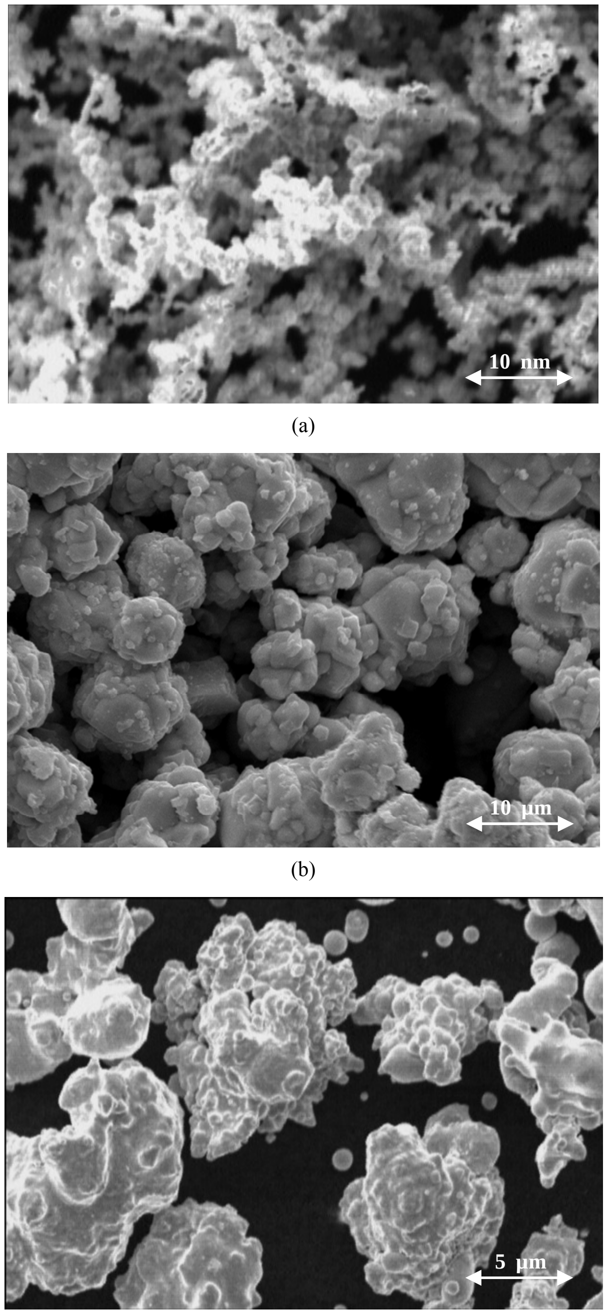

(a) (b) (c)

Figure 1. The morphology of a) Nano ZrO_2, b) Micron ZrO_2 and c) WC powders.

Table 1. The amount of WC and ZrO_2 for production of a 150 g workpiece.

Code of Sample	WC to ZrO_2 molar ratio	Particle Size	WC + ZrO_2 (g)	WC (g)	ZrO_2 (g)
3W1Z-M	3:1	Micron	150	124	26
3W1Z-N	3:1	Nano	150	124	26

regarding the desired proportion of W to ZrC in composite this ratio may be different. After 6 hours mixing in alcohol media, the resulting mixture is dried 12 hours in an oven. Finally this mixture is gelcasted to make a preform from WC and ZrO_2 powder [15-18]. The gelcasting was done according to the steps showing in **Figure 2**, in which sodium alginate ($C_6H_7NaO_6$), sodium hexametaphosphate ($(NaPO_3)_6$), phosphate calcium ($Ca_3(PO_4)_2$) and ammonium citrate ($(NH4)_3C_6H_5O_7$) were used as monomers and after adding each of them mixing continues for 10 minutes. Then the mixture of WC and ZrO_2 were added slowly and finally hexane acid ($C_6H_{10}O_4$) was added as initiator, that at this stage the workpiece must be casted quickly before hardening. The mold used here is made of rubber which compared with other materials and offered the best results.

The workpiece remains 24 hours at room temperature, heated 6 hours in an oven at 50 - 60˚C to burn polymeric additives and then for calcination, it is pulled out from the mold and heated in a vacuum furnace at 600 - 700˚C. The last step is sintering that usually is done at about 1500˚C. **Figure 3** shows the sintering process for gel casting. The gel casted body is sintered in a vacuum furnace at 2100˚C [13], according to the cycle showing in **Figure 4**.

In order to detect the type of synthesized phases and components XRD analysis with the Cu Kα radiation (λ = 1.54 Å) was carried out and the integrated area of the

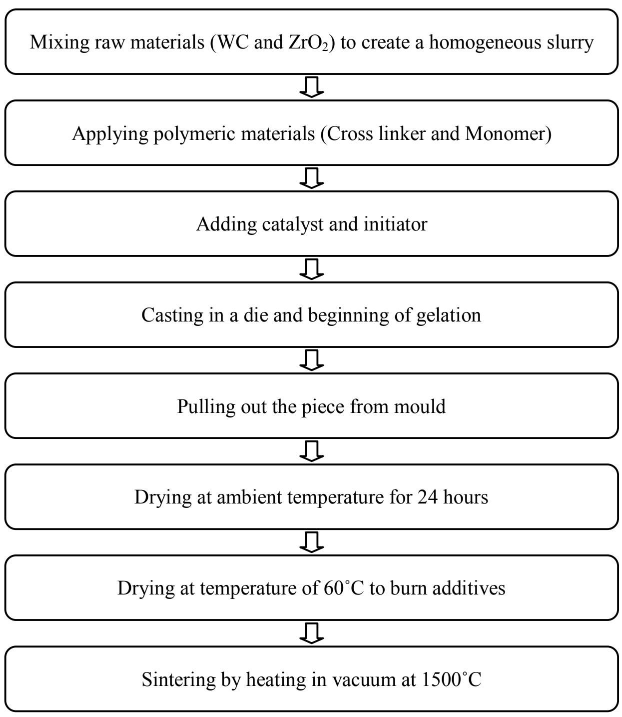

Figure 2. The steps in gel casting of WC/ZrO_2.

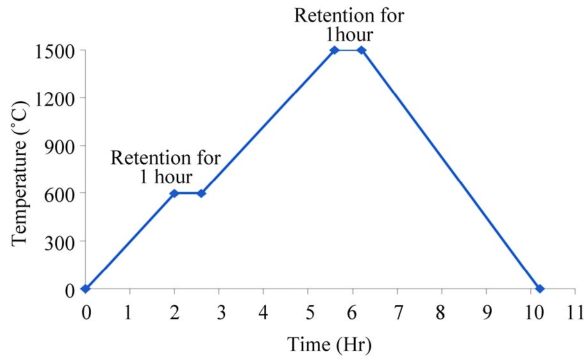

Figure 3. The sintering process of gel casting.

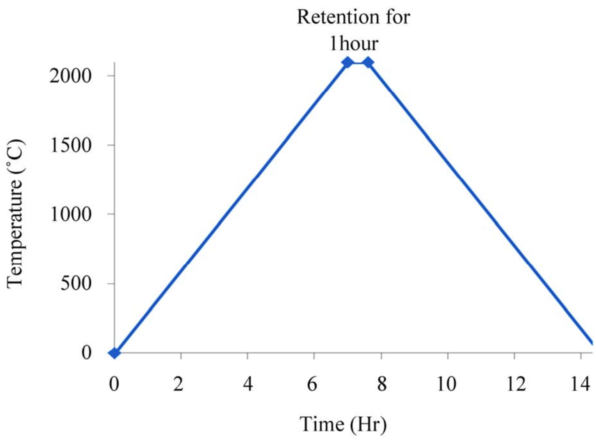

Figure 4. The sintering process of reaction sintering.

peaks were calculated to obtain the volume fraction of the phases in the composite. Additionally the microstructure of the samples was studied using scanning electron microscope. To see the differences between phases in the composites, the back scattered electron (BSE) images were studied as well as secondary electron (SE) images.

3. Results and Discussion

To control the formation of W-ZrC composite x-ray diffraction of the powders before reaction and after making the composites were analyzed to see whether the reaction is complete or not. **Figure 5** shows the XRD pattern of composite made from micron powders (3W1Z-M) and **Figure 6** shows the XRD pattern of composite made from nano powders (3W1Z-N) in which 1) is WC powder, 2) ZrO_2 powder, 3) The mixture of WC and ZrO_2 and 4) W-ZrC composite.

Figure 5 is the XRD pattern of 3W1Z-M sample, showing the peaks belong to ZrC and W phases that confirms the formation of W/ZrC composite was successful. In spite of that some WC and ZrO_2 phases are observed which illustrates that reaction between these two phases to form W/ZrC composite was not complete. Also the W2C phase that was formed during mixing, still exist in the composite. According to the integrated area of the peaks related to these phase and the total XRD patterns, the volume fraction of them is calculated and listed in **Table 2**.

Figure 6 is the XRD pattern of 3W1Z-N sample. In this pattern ZrC and W phases are visible that point out the formation of W/ZrC composite through reaction sintering. On the other hand some ZrO_2 phase is observed but there is no WC any more. The W_2C phase still exists in the composite. According to the integrated area of peaks in the XRD patterns, the volume fractions of these phases are shown in **Table 3**.

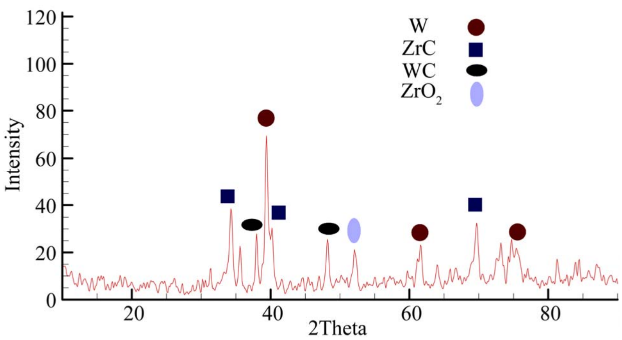

Figure 5. XRD pattern of composite fabricated by reaction sintering of micron WC/ZrO_2.

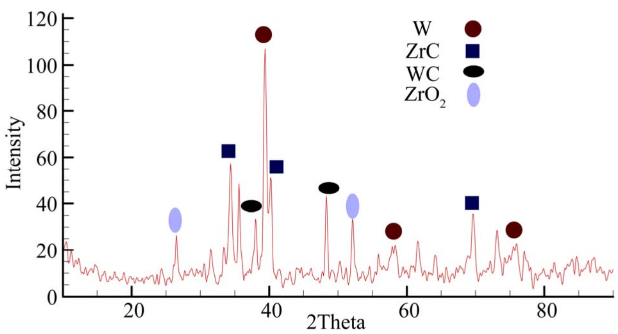

Figure 6. XRD pattern of composite fabricated by reaction sintering of nano WC/ZrO_2.

Table 2. The volume fraction of different phases in the 3W1Z-M Sample.

Phase	W	ZrC	ZrO_2	WC	W_2C
Vol%	40.1	19.7	10.2	9.1	20.9

Table 3. The volume fraction of different phases in the 3W1Z-N sample.

Phase	W	ZrC	ZrO_2	W_2C
Vol%	45.1	24.7	10.9	19.3

Finally by SEM micrographs the morphology of the samples is studied. **Figure 7** shows the BSE micrograph of W-ZrC composite and **Figure 8** shows the BSE micrograph in 3W1Z-N sample.

As it is clear the bright phase in back scattered electron images related to heavier elements. On the other hand in the images, the composite is made of a dark phase and a bright phase which represent zirconium carbide and tungsten respectively. To prove this EDX-line scan of both phases were studied. **Figure 9** shows the EDX-line scan of bright phase and dark phase in W/ZrC composite. Accordingly in 3W1Z-N sample the amount of W is more, that shows the reaction in nano powder improved better.

The average values for mechanical properties of the both nano and micron samples, including density, hardness, Elastic modulus and Flexural strength, are listed in

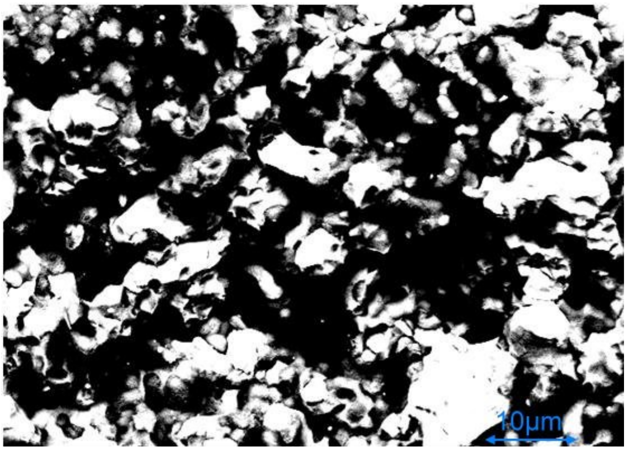

Figure 7. The BSE micrograph of W/ZrC composite prepared by reaction sintering in 3W1Z-M sample.

Figure 8. The BSE micrograph of W/ZrC composite prepared by reaction sintering in 3W1Z-N sample.

Table 4 Comparing to prior ZrC-W composites [2] these values for mechanical properties are acceptable. Anyway the variances might be because the reaction between ZrO_2 and WC did not go to completion and because of the effect that the un-reacted components have on the properties of the composite.

4. Conclusions

In this study the feasibility of fabricating W/ZrC composite through reaction sintering was studied and the differences of composite made from nano and micron ZrO_2 were investigated. The W/ZrC composite was produced by mixing WC and ZrO_2 powders, gel casting the mixture to produce a green body and then sintering at 2100˚C. The XRD patterns and SEM images indicate that W/ZrC composite has been fabricated successfully by this method, although some extra compounds have been formed. Moreover the XRD pattern of nano sample showed that the reaction was more successful and proceeded more effectively, with regard to ~45%W-25%ZrC in nano sample compared to ~40%W-20%ZrC in micron sample. Additionally the amount of unreacted ZrO_2 decreases and there remains no WC in nano sample. The amount of unwanted W2C phase decreases as well. Even when some weak points, like the inefficiency of process and presence of ZrO_2 phase, were taken to consideration, the produced composites showed good mechanical properties, comparable to the composites fabricated through hot-press and other conventional methods. Anyway the composite produced by nano powders possess better properties rather than the micron one.

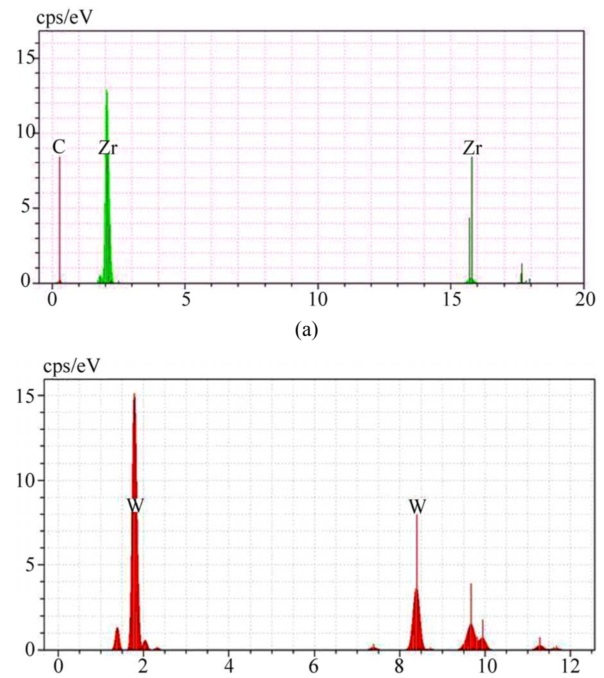

Figure 9. EDX-line scan of (a) Dark phase and (b) Bright phase in 3W1Z-N sample.

Table 4. The mechanical properties and standard deviation for made W/ZrC composites.

Sample	Density (g/cm^3)	Hardness (GPa)	Elastic modulus (GPa)	Flexural strength (MPa)
3W1Z-M	12.1	4.3	339	431
3W1Z-N	12.8	4.7	368	442

5. Acknowledgements

The authors would like to express their gratitude to Dr. Y. Vahidshad in writing the article and useful discussion and suggestion in this study and M. Hajizamani for providing language help.

REFERENCES

[1] T. Zhang, Y. Wang, Y. Zhou and G. Song, "Compressive Deformation Behavior of a 30 vol.%ZrCp/W Composite at Temperatures of 1300-1600˚C," *Materials Science and Engineering A*, Vol. 474, No. 1-2, 2008, pp. 382-389. doi:10.1016/j.msea.2007.04.024

[2] M. Roosta and H. Baharvandi, "The Comparison of W/Cu and W/ZrC Composites Fabricated through Hot-Press," *International Journal of Refractory Metals and Hard Materials*, Vol. 28, No. 5, 2010, pp. 587-592. doi:10.1016/j.ijrmhm.2010.04.006

[3] B. Dickerson, P. J. Wurm, J. R. Schorr, W. P. Hoffman, P. G. Wapner and K. H. Sandhage, "Near Net Shape Ultra High Melting Recession Resistant ZrC/W-Based Rocket Nozzle Liners via the Displacive Compensation of Porosity (DCP) Method," *Journal of Materials Science*, Vol. 39, No. 19, 2004, pp. 6005-6015. doi:10.1023/B:JMSC.0000041697.67626.46

[4] P. Kumar and K. H. Sandhage, "The Displacive Compensation of Porosity (DCP) Method for Fabricating Dense, Shaped, High-Ceramic-Bearing Bodies at Modest Temperatures," *Journal of Materials Science*, Vol. 34, No. 23, 1999, pp. 5757-5769. doi:10.1023/A:1004754117195

[5] T. Zhang, Y. Wang, Y. Zhou, T. Lei and G. Song, "Effect of Temperature Gradient in the Disk during Sintering on Microstructure and Mechanical Properties of ZrCp/W Composite," *International Journal of Refractory Metals and Hard Materials*, Vol. 27, No. 1, 2009, pp 126-129. doi:10.1016/j.ijrmhm.2008.05.005

[6] G. Song, Y. Wang and Y. Zhou, "The Mechanical and Thermophysical Properties of ZrC/W Composites at Elevated Temperature," *Materials Science and Engineering A*, Vol. 334, No. 1-2, 2002, pp. 223-232. doi:10.1016/S0921-5093(01)01802-0

[7] T. Zhang, Y. Wang, Y. Zhou, T. Lei and G. Song, "Ele-

vated Temperature Compressive Failure Behavior of a 30 vol.%ZrCp/W Composite," *International Journal of Refractory Metals and Hard Materials*, Vol. 25, No. 5-6, 2007, pp. 445-450. doi:10.1016/j.ijrmhm.2006.06.001

[8] G. Song, Y. Wang and Y. Zhou, "Effect of Carbide Particles on the Ablation Properties of Tungsten Composites," *Materials Characterization*, Vol. 50, No. 4-5, 2003, pp. 293-303. doi:10.1016/S1044-5803(03)00123-2

[9] G. Song, Y. Wang and Y. Zhou, "Thermo Mechanical Properties of TiC Particle-Reinforced Tungsten Composites for High Temperature Applications," *International Journal of Refractory Metals and Hard Materials*, Vol. 21, No. 1-2, 2003, pp. 1-12. doi:10.1016/S0263-4368(02)00105-1

[10] G. Song, Y. Wang and Y. Zhou, "The Microstructure and Elevated Temperature Strength of Tungsten-Titanium Carbide Composite," *Journal of Materials Science*, Vol. 37, No. 16, 2002, pp. 3541-3548. doi:10.1023/A:1016583611632

[11] G. Song, Y. Wang, Y. Zhou and T. Lei, "Elevated Temperature Strength of a 20 vol% ZrCp/W Composite," *Journal of Materials Science Letters*, Vol. 17, No. 20, 1998, pp. 1739-1741. doi:10.1023/A:1006639606300

[12] G. Song, Y. Wang and Y. Zhou, "Elevated Temperature Ablation Resistance and Thermo Physical Properties of Tungsten Matrix Composites Reinforced with ZrC Particles," *Journal of Materials Science*, Vol. 36, No. 19, 2001, pp. 4625-4631. doi:10.1023/A:1017989913219

[13] S. C. Zhang, G. E. Hilmas and W. G. Fahrenholtz, "Zirconium Carbide-Tungsten Cermets Prepared by *in Situ* Reaction Sintering," *Journal of the American Ceramic Society*, Vol. 90, No. 6, 2007, pp. 1930-1934. doi:10.1111/j.1551-2916.2007.01642.x

[14] L. J. Lin, G. Z. Ren, M. P. Chen and Y. Liu, "The Behavior of Er^{3+} Dopant during Crystallization in Oxyfluoride Silicate Glass Ceramics," *Journal of Alloys and Compounds*, Vol. 486, No. 1-2, 2009, pp. 261-264. doi:10.1016/j.jallcom.2009.05.154

[15] M. Roosta, H. Baharvandi and H. Abdizade, "The Evaluation of W/ZrC Composite Fabricated through Reaction Sintering of Two Precursors: Conventional ZrO_2/WC and Novel $ZrSiO_4$/WC," *International Journal of Refractory Metals and Hard Materials*, IJRMHM-D-11-00040R1. (In Press)

[16] M. Kokabi, A. A. Babaluo and A. Barati, "Gelation Process in Low-Toxic Gelcasting Systems," *Journal of the European Ceramic Society*, Vol. 26, No. 15, 2006, pp. 3083-3090. doi:10.1016/j.jeurceramsoc.2005.08.020

[17] M. D. Vlajic and V. D. Krstic, "Strength and Machining of Gelcast SIC Ceramics," *Journal of Materials Science*, Vol. 37, No. 14, 2002, pp. 2943-2947. doi:10.1023/A:1016064913446

[18] Y. Li and Z. M. Guo, "Gelcasting of WC-8 wt%Co Tungsten Cemented Carbide," *International Journal of Refractory Metals and Hard Materials*, Vol. 26, No. 5, 2008, pp. 472-477. doi:10.1016/j.ijrmhm.2007.11.003

New Journal of Glass and Ceramics, **2011, 1, 7-12**
doi:10.4236/njgc.2011.11002 Published Online April 2011 (http://www.SciRP.org/journal/njgc)

Effect of Aging on Chlorophyll Species Embedded in Silica Xerogels Matrix

José R. Martínez[1*], Erika Espericueta[1,2], Gerardo Ortega-Zarzosa[1]

[1]Universidad Autónoma de San Luis Potosí, San Luis Potosí, México;
[2]Centro de Investigación en Materiales Avanzados, Chihuahua, México.
Email: flash@fciencias.uaslp.mx

Received February 16th, 2011; revised March 30th, 2011; accepted April 6th, 2011.

ABSTRACT

The spectral fluorescence characteristics of extracts leaves embedded in silica xerogel matrix promoted by aged time was studied. We obtain a higher PSII stability for extract of leaves embedded in xerogel matrix, with concentration of 8 *g* / 20 *ml and water to TEOS molar ratio of* 11, *which remain bioactive over a very long period of time, whereas for a water to TEOS molar ratio of* 5 *a blue-shift fluorescence is observed indicating the PSII denaturizing and formation of fluorescing aggregates associated with the activation of carotenoids radicals.*

Keywords: *Fluorescence Spectra, Sol-Gel, Chlorophyll, Extract Leaves, Photosystem II*

1. Introduction

Sol-gel has even been used to encapsulate and maintain the activity of biomolecules. However, currently investigation about organically-modified sol-gels in an effort to control overall dopant mobility, accessibility, and reactivity are made in the present.

The number of potential applications of organic doped sol-gel glasses is very large; important possibilities include optics and electro-optics. Development of these applications requires a good understanding of the structure of the doped sol-gel matrices, the properties of the matrices on the molecular level and the conditions that the oxide network imposes on the optical properties of the dopant [1].

Sol-gel technique with the ability to trap photoactive substances in an inorganic gel glass, has led to some new applications in nonlinear optics, solid-state tunable lasers, photochemical hole burning, etc [2,3].

Metalloporphyrin complexes have received much attention owing to their important role in biology, solar energy conversion, photonics, and catalysis [4]. Spectroscopic evidence confirmed stability of the dispersion over a period of three to four months.

As an optical substance adsorbed into an inorganic matrix, chlorophyll and composites based in chlorophyll has been poorly studied, in spite of the interesting applications of chlorophyll's optical properties [5-7].

The higher plants are an efficient system to absorb and transfer the energy through photosynthetic apparatus. This situation can be used to take advantage to prepare materials based in extract of plants for eventually design efficient optical- and electrooptical-based sol-gel encapsulated biomolecules [8].

The immobilization of organic pigments on inorganic media may be useful for the design of energy conversion devices [9].

Thus, it is necessary to understand the structural evolution of extracted components of leaves embedded in silica xerogel matrix, as well as the interaction between the pigments embedded into the inorganic matrix.

The typical fluorescence spectrum of green plants, embedded or not embedded in xerogel matrix, is in the range from 650 nm to 780 nm, presenting two maximum of fluorescence located at about 670 nm and 730 nm corresponding to chlorophyll *a* and at about 650 nm and 710 nm corresponding to chlorophyll *b* [8,10].

All green plants contain chlorophyll *a* and chlorophyll *b* in their chloroplast. In higher plants, chlorophyll *a* is the major pigment and chlorophyll *b* is an accessory pigment, and the *a*/*b* ratio is generally around 3 to 1 [11]. Chlorophyll *b* differs from chlorophyll *a* by having an aldehyde (–CHO) group instead of a methyl group ($–CH_3$).

The differences in these structures cause that the two maximum of fluorescence of chlorophyll *a* are located at 670 nm and 730 nm, while the two maximum of fluorescence of chlorophyll *b* are at 650 nm and 710 nm [10,12].

The green plants contain the photosystem I and II (PSI, PSII). A photosystem consist of a peripheral antenna or ligh-harvesting complex, an inner antenna and the reaction center. The Photosystem II is the principal system in which the electron transfer in the photosynthesis process occur.

Chlorophyll is present in the two photosystems, PSI and PSII, but only photosystem II has additional minor chlorophyll *a*/*b* binding antenna protein. Both photosystems differ in their absorption and fluorescence characteristic. The maximum of fluorescence intensity can be found for PSI at 735 nm and PSII at 683 nm. At room temperature it can be assumed that all variable fluorescence originates from PSII [10,13].

The photosystem PSII can be monitoring by chlorophyll *a* fluorescence. Thus the observed maximum intensity fluorescence, corresponding to excitation energy transfer to the photosystem II, is at about 683 nm [8].

Metal porphyrins are molecules present in nature, such leaves, for example the magnesium porphyrin in chlorophyll. The components of the complex extracted of leaves includes the chlorophyll, which is the principal component in most green plants, but exist in the Photosystem II at least 25 different types of protein subunits, PSII is a large supramolecular pigment-protein complex embedded in the thylakoid membranes of green plants.

In previous works we show that the samples with extract of leaves embedded in silica xerogel matrix show that PSII chlorophyll fluorescence transients is non present and the samples show a higher PSII thermostability for leaves embedded in xerogel matrix than in the green leaves [8,14].

Under heat treatment, the original bands located at about 670 and 714 nm observed in the fluorescence spectrum, are substituted by a blue-shifted band at about 580 nm. These changes can be attributed to the tight environment around the chlorophyll and to the different polarity of the environment inside the pores of the silica matrix, among the conversion of chlorophyll to protein species, as phaeophytene [15,16].

The large shift is typical for weakening of chlorophyll – protein interactions in pigment – protein complex (PPCs). One may assume that the observed spectral changes are associated with changes of spectral distortion in the pigments embedded in silica xerogel matrix during heat treatment, due to the structural evolution of the matrix.

In this work, by measurements of the PSII fluorescence comportment, we report biostability of sol-gel amorphous bulk samples containing extract of spinach leaves which is sensitive to concentration of the aggregates.

2. Experimental Procedure

The standard method to extract compound of leaves is by crude extraction from frozen leaves, washed with water, by simple grinding and mixing them with ethanol solvent. For the extraction three arbitrary concentrations, 4 g, 8 g and 50 g of leaves for 20 ml of ethanol, corresponding to low, medium and very high concentration, were used, in order to obtain information about the effect of concentration in the aging process. The solution of ethanol and extract was centrifuged at 3000 rpm for 5 minutes and then filtered with a Wattsman filter nr. 1.

In order to obtain the organic composites of extract of leaves embedded in xerogel matrix, a precursor material composed of TEOS, water, and ethanol with pigments extract of leaves, of spinach was prepared. The set of samples were prepared using a constant ethanol to TEOS molar ratio of 4:1 and a molar ratio of water to TEOS (R) of R = 11 and R = 5. These quantities correspond to a high water/TEOS ratio, needed to enhance the hydrolysis to assure a close amorphous structure for the as-prepared SiO_2 powder [17]. The TEOS was dissolved in the ethanol with pigments using magnetic stirring for 15 min and then the water was added to the ethanol-TEOS solution using magnetic stirring for 10 minutes to form the starting material. The pH of the final solution was 5.

Soft pieces of the gel were obtained after 48 hr. Those pieces were ground to form a fine powder.

The emission spectra measurements were carried out in a fluorescence spectrometer by Ocean Optics Inc. model SF2000 using a reflectance diffuse 45˚ configuration using a double fiber optic component, excited with an Omnicrome argon ion laser of 532 nm and filter HNF-532-1.0, in order to obtain the fluorescence contribution due to the photosystem II of samples measured after gelling and for the same samples measured after 36 months of gelling.

In order to get similar grain size the samples were ground to form fine powder; the experimental set up to obtain emission spectra measurement was regularly used for compared spectroscopy measurement, such NIR, Raman and fluorescence, obtained in the same experimental condition, in this case by relative intensity fluorescence.

3. Results and Discussion

In order to investigate the structural and fluorescence change, the set of samples with different extract concentration were irradiate with 532 nm laser using the diffuse reflectance, the fluorescence results obtained are shown in the next figures.

Figures 1-3, shows the fluorescence spectra for silica xerogel with 4 g, 8g and 50 g per 20 ml of extract spinach leave with R = 11, respectively. The as-prepared samples present the typical chlorophyll *a* fluorescence (range from 650 nm to 780 nm) in which no change of fluorescence characteristic occurred with aged time increasing. For **Figures 1** and **3**, a blue-shift of the spectra is observed when the aged time is increased at 36 months and the maximum fluorescence shift from 678 nm to 669 nm, and 686 nm to 675 nm, after 36 month, respectively, whereas for **Figure 2**, the maximum fluorescence is unchanged maintenance at 678 nm. In the latest case we obtain a great biostability for such formation parameters. When the ratio R is reduced to R = 5, maintaining the concentration of 8 g / 20 ml the biostability is breaking as we can observed in **Figure 4**. For this sample the aged effect decomposes the chlorophyll contribution and a denaturalization occurs as we discuss in next paragraph.

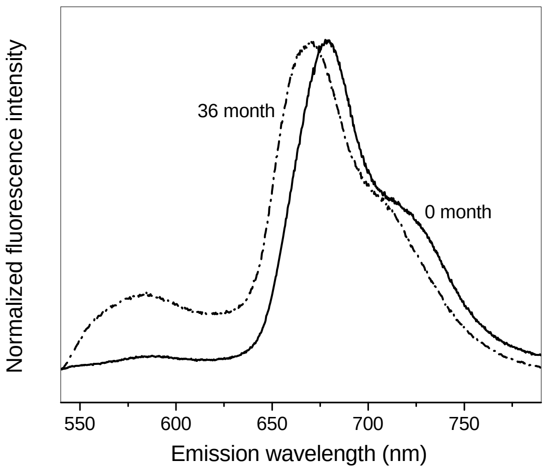

Figure 1. Fluorescent emission spectra of spinach leaves, with concentration of 4 g / 20 ml, embedded in silica xerogel matrix measured after gelling and after 36 months of gelling.

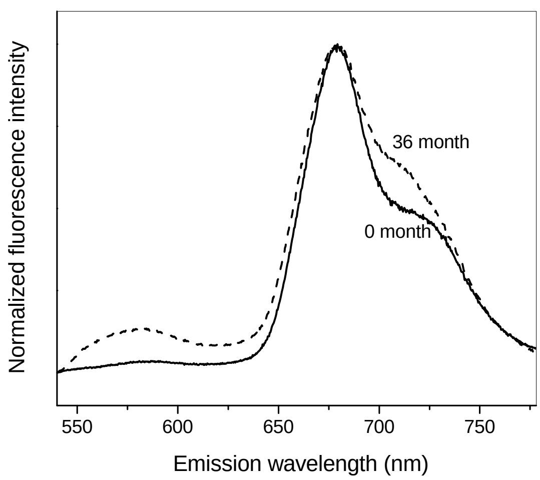

Figure 2. Fluorescent emission spectra of spinach leaves, with concentration of 8 g / 20 ml, embedded in silica xerogel matrix measured after gelling and after 36 months of gelling.

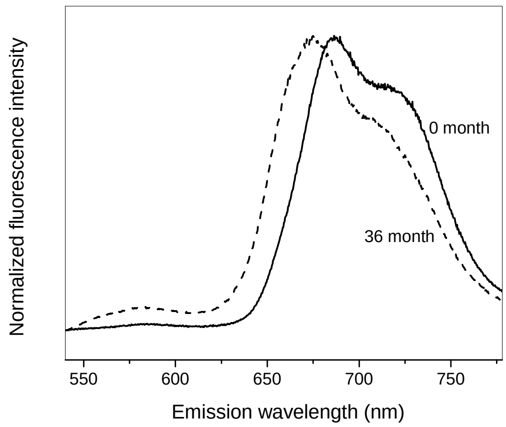

Figure 3. Fluorescent emission spectra of spinach leaves, with concentration of 50 g / 20 ml, embedded in silica xerogel matrix measured after gelling and after 36 months of gelling.

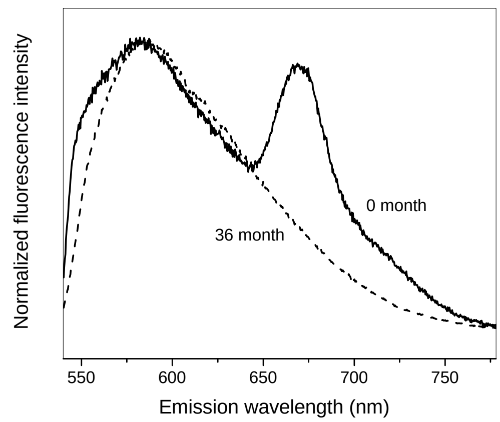

Figure 4. Fluorescent emission spectra of spinach leaves, with concentration of 4 g / 20 ml and water to TEOS molar ratio of 5, embedded in silica xerogel matrix measured after gelling and after 36 months of gelling.

Figure 2 shows there is not significant change of fluorescence of chlorophyll entrapped in silica xerogel up to 36 months, revealing unchanged in chlorophyll structure, in samples where extracted leaves of spinach were embedded in silica xerogel, thus the chlorophyll *a* molecules remain structurally same in silica xerogel over a very long period of time. In particular the maximum position of fluorescence of the PSII unchanged in terms of sol-gel aging time. This time period is very long compared with time, about 3 months, reported in work where chlorophyll *a* molecules was entrapped in silica gel nanomatrix [16].

This results contrast with the case of barley leaves embedded in silica xerogel matrix where a 10 nm blue shift of the red emission maximum after aging for about 12 months was observed [8].

In conclusion extract of spinach leaves with concentration of 8 g / 20 ml and R = 11 embedded in silica xerogel matrix present a higher PSII biostability, remaining bioactive over very long periods of time.

Thus the formation of biostable compound, for very long aged times, of chlorophyll species embedded in silica xerogel can be obtained by controlling concentration of extract leave and ethanol to TEOS and water to TEOS molar ratios.

In **Figure 1** where a 9 nm shift of maximum fluorescence is observed, which can be associated with changes of spectral distortion in the pigments embedded in silica xerogel matrix during the aged, due to the structural evolution of the matrix. The shift is attributed also to changes of the tight environment around the chlorophyll and to the different polarity of the environment inside the pores of the silica matrix, among the conversion of chlorophyll to protein species, as phaeophytene [15,16]. Indicate us that, among the previous assignment for the fluorescence blue shift, denaturations of chlorophyll species occur with a increasing of chlorophyll *b* respect to chlorophyll *a*.

Figure 2, represent a biostabilizing system in which the chlorophyll *a* don't decompose to phaeophytene and only a little increase of chlorophyll *b* is observed when the aged time increasing indicated by an increase in the fluorescent intensity with a wave length shift of the band located at 726 nm to 713 nm.

In **Figure 3**, we show the sample with a high extract leave concentration. In this case a pigment aggregation is present and then a red shift of maximum fluorescent, respect to 675 nm obtained for the samples with 4 g and 8 g per 20 ml of extract leave concentration. The maximum fluorescence is located at 686 nm. The band located at 724 nm present a higher intensity compared with samples of **Figures 1** and **2**, corresponding to low extract leave concentration.

When the water to TEOS molar ratio is reduced the biostabilization is breaking as we can observe in **Figure 4**, where the fluorescent spectra for an extract leave concentration of 8 g / 20 ml and water to TEOS molar ratio of 5 is shown.

The fluorescent contribution between 630 nm to 750 nm corresponds to chlorophyll *b* with bands located at 668 nm and 710 nm characteristic of such chlorophyll specie. The aging effect produce a rapid denaturation of chlorophyll compound and a blue shift occur. The typical red fluorescence disappear and a blue-shifted band at about 580 nm is present [14], indicating the decomposition of the photosystem II. This situation is also observed in samples of ortho-amnino-substituted porphyrin, $H_2T(o\text{-}NH_2)PP$, embedded in SiO_2 matrix [15].

The large shift is typical for weakening of chlorophyll – protein interactions in pigment – protein complex (PPCs). The carotenoid radical cation formation play one important role in photosynthetic pigment-protein complexes, and quench chlorophyll fluorescence [18,19]. The chlorophyll molecule contain the phytyl group associated to carotenoid radical, the low water content retarding the gel formation and the denaturation of photosystem II active the carotenoid function of protect the photosynthetic apparatus by quenching chlorophyll triplet state which inhibits the formation of singlet state oxygen [20-22], and stabilize light-harvesting protein structures [23-25]. The active presence of carotenoid radicals is indicated by the blue shift band located at 583 nm [26].

The difference in structure due to concentration of extract leave and water to TEOS molar ratio, are reflected on the fluorescence differences discussed previously. In **Figure 5** we observe that, among the differences in relative intensities for bands characteristic of chlorophyll *a* and *b*, related with the photosystems I and II, we observe that the position of maximum fluorescence of the band corresponding to PSII at about 680 nm, is red shifted conform the concentration is increased. This result is in agreement with results reported by Furukawa *et al.*, for layered silica/surfactant mesostructured this films containing chlorophyllous pigments where the red shift in optical measurements indicates the aggregation of pigments [9].

The fluorescent bands, for samples labeled by C1 and C2 concentrations in **Figure 5** are very similar, with a lighter red shift for sample C2 respect to C1. However for aged samples these bands present higher differences indicating that a higher biostabilisation is obtained for concentration C2, as we can observe in **Figure 6**.

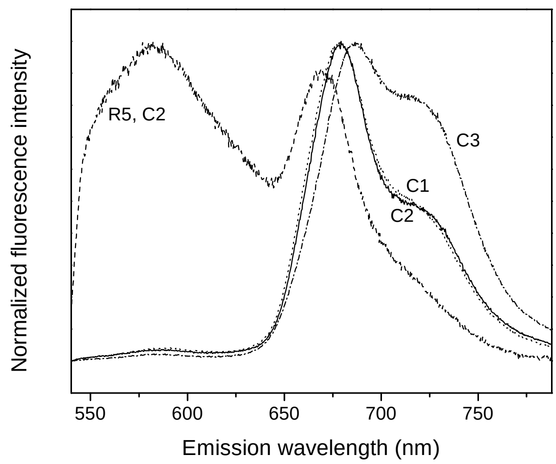

Figure 5. Fluorescent emission spectra of spinach leaves, with concentration of 4 g / 20 ml (C1), 8 g / 20 ml (C2), 50 g / 20 ml (C3) and 8 g / 20 ml with water to TEOS molar ratio of 5 (R5,C2), embedded in silica xerogel matrix measured after gelling.

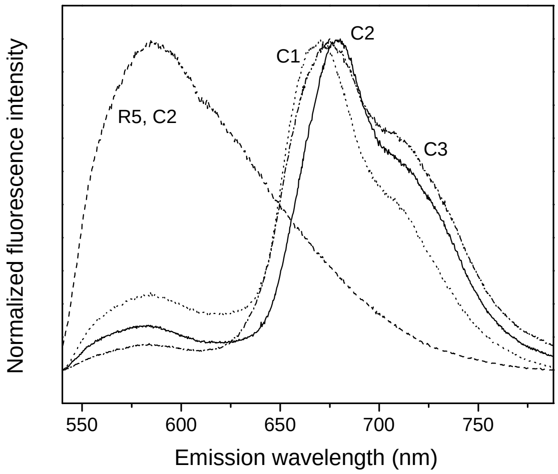

Figure 6. Fluorescent emission spectra of spinach leaves, with concentration of 4 g / 20 ml (C1), 8 g / 20 ml (C2), 50 g / 20 ml (C3) and 8g / 20ml with water to TEOS molar ratio of 5 (R5,C2), embedded in silica xerogel matrix measured after 36 months of gelling.

4. Conclusions

The PSII fluorescence comportment for spinach extract of leaves embedded in silica xerogel matrix, give us information about the microstructural evolution during the silica-gel-glass conversion.

We obtain a higher PSII stability for extract of leaves, with concentration of 8 g / 20 ml and water to TEOS molar ratio of 11.67 embedded in xerogel matrix, which remain bioactive over a very long period of time, whereas for a water to TEOS molar ratio of 5 a blue-shift fluorescence is observed indicating the PSII denaturizing and formation of fluorescing aggregates associated with the activation of carotenoids radicals.

In samples with a water to TEOS molar ratio of R = 11, and concentration between 4 g to 50 g per 20 ml the chlorophylls molecules entrapped in silica xerogel remain bioactive over a long period of time.

REFERENCES

[1] D. Levy, "Organic Doped Sol-Gel Glasses for Electro-Optics and Display Applications," *Pure & Applied Optics*, Vol. 5, No. 5, 1996, pp. 621-629. doi:10.1088/0963-9659/5/5/016

[2] J. D. Mackenzie and D. R. Ulrich, "Sol-Gel Optic 1," *Proceedings of SPIE*, Washington, Vol. 1328, 1990, pp. 2-13. doi:10.1117/12.22540

[3] G. Qian and M. Wang, "Study on the Microstructural Evolution of Silica Gel During Sol-Gel-Gel-Glass Conversions Using the Fluorescence Polarization of Rhodamine B," *Journal of Physics D: Applied Physics*, Vol. 32, No. 18, 1999, pp. 2462-2466. doi:10.1088/0022-3727/32/18/320

[4] A. Ghosh, T. Selvamani, D. Amilan, A. Das and I. Mukhopadhyay, "Generation of Nanostructures by the Aggregation of Porphyrin Derivatives with Long Alkane Chain in Mix-Solvent," *Journal of Nanomaterials*, Vol. 2007, No. 1, 2007, 8 pages.

[5] J. Ramírez-Niño, C. Pérez-Abad, J. Rodríguez, J. García, M. Castaño and V. M. Castaño, "Optical Properties of Chlorophyll-Doped Silica Gels," *Journal of Materials Science*: *Materials in Electronics*, Vol. 8, No. 1, 1997, pp. 1-5.

[6] S. Sathyendranath, F. E. Hoge, T. Patt and R. N. Swift, "Detection of Phytoplank-Ton Pigments From Ocean Color: Improved Algorithms," *Applied Optics*, Vol. 33, No. 6, 1994, pp. 1081-1089.

[7] R. B. Myneni, F. G. Hall, P. J. Sellers and A. L. Marshak, "The Interpretation of Spectral Vegetation Indexes," *IEEE Transactions on Geoscience and Remote Sensing*, Vol. 33, No. 2, 1995, pp. 481-486. doi:10.1109/36.377948

[8] A. Vázquez-Durán, C. Araujo-Andrade, G. Martínez-Castañón, G. Ortega-Zarzosa, F. Ruiz and J. R. Martínez, "Spectral Characterization of Chlorophyll Fluorescence in Extract of Barley Leaves Embedded in Silica Xerogel Matrix," *Journal of Sol-Gel Science and Technology*, Vol. 39, No. 3, 2006, pp. 223-227.

[9] H. Furukawa, N. Inoue, T. Watanabe and K. Kuroda, "Energy Transfer between Chlorophyll Derivatives in Silica Mesostructured Films and Photocurrent Generation," *Langmuir*, Vol. 21, No. 9, 2005, pp. 3992-3997. doi:10.1021/la047845z

[10] J. M. Briantais, C. Vernotte, G. H. Krause and E. Weiss, "In Light Emission by Plants and Bacteria," Academic Press, New York, 1986.

[11] J. Gross, "Pigment in Vegetables: Chlorophyll and Carotenoids," Van Nostrand Reinhold, New York, 1991.

[12] R. Stefen, "Time-Resolved Spectroscopic Investigation of Photosystem II," Thesis: Doktor der Naturwissenchaften, Technischen Universität, Berlin, 2003.

[13] N. R. Baker and A. N. Webber, "Interactions between Photosystems," *Advances in Botanical Research*, Vol. 13, 1987, pp. 1-66. doi:10.1016/S0065-2296(08)60340-7

[14] J. M. Guajardo-Pacheco, G. Ortega-Zarzosa and J. R. Martínez, "Fluorescents Effects of Silica Xerogel Induced by Incorporation of Chard Leaves Extracts and ZnO Nanoparticles," *Superficies y Vacio*, Vol. 21, No. 1, 2008, pp. 16-19.

[15] M. A. García-Sánchez, S. R. Tello, R. Sosa and A. Campero, "Fluorescent Porphyrins Trapped in Monolithic SiO_2 Gels," *Journal of Sol-Gel Science and Technology*, Vol. 37, No. 2, 2006, pp. 93-97.

[16] J. S. Manna, S. Basu, M. K. Mitra, S. Mukherjee and G. C. Das, "Study on the Biostability of Chlorophyll *a* Entrapped in Silica Gel Nanomatrix," *Journal of Materials Science*: *Materials in Electronics*, Vol. 20, No. 11, 2009, pp. 1068-1072. doi:10.1007/s10854-008-9827-6

[17] J. R. Martínez, F. Ruiz, Y. V. Vorobiev, F. Pérez-Robles and J. González-Hernández, "Infrared Spectroscopy

Analysis of the Local Atomic Structure in Silica Prepared by Sol-Gel," *Journal of Chemical Physics*, Vol. 109, No. 17, 1998, pp. 7511-7514.

[18] H. A. Frank and G. W. Brudvig, "Redox Functions of Carotenoids in Photosynthesis," *Biochemistry*, Vol. 43, 2004, pp. 8607-8615. doi:10.1021/bi0492096

[19] D. Phillip, A. V. Ruban, P. Horton, A. Asato and A. J. Young, "Quenching of Chlorophyll Fluorescence in the Major Light-Harvesting Complex of Photosystem II: A Systematic Study of the Effect of Carotenoid Structure," *Proceedings of the National Academy of Sciences*, Vol. 93, 1996, pp. 1492-1497. doi:10.1073/pnas.93.4.1492

[20] C. S. Foote, "Mechanisms of Photosensitized Oxidation," *Science*, Vol. 162, No. 3857, 1968, pp. 963-970. doi:10.1126/science.162.3857.963

[21] G. Renger and C. Wolff, "Further Evidence for Dissipative Energy Migration via Triplet States in Photosynthesis. The Protective Mechanism of Carotenoids in Rhodopseudomonas Spheroides Chromatophores," *Biochimica et Biophysica Acta* (*BBA*)—*Bioenergetics*, Vol. 460, No. 1, 1977, pp. 47-57.

[22] F. Boucher, M. van der Rest and G. Gingras, "Structure and Function of Carotenoids in the Photoreaction Center from Rhodospirillum Rubrum," *Biochimica et Biophysica Acta* (*BBA*)—*Bioenergetics*, Vol. 461, No. 3, 1977, pp. 339-357.

[23] H. P. Lang and C. N. Hunter, "The Relationship between Carotenoid Biosynthesis and the Assembly of the Light-Harvesting LH2 Complex in Rhodobacter Sphaeroides," *Biochemical Journal*, Vol. 298, No. 1, 1994, pp. 197-205.

[24] D. Sandonà, R. Croce, A. Pagano, M. Crimi and R. Bassi, "Higher Plants Light Harvesting Proteins. Structure and Function as Revealed by Mutation Analysis of Either Protein or Chromophore Moieties," *Biochimica et Biophysica Acta* (*BBA*)—*Bioenergetics*, Vol. 1365, No. 1-2, 1998, pp. 207-214.

[25] H. Yamamoto and R. Bassi, "Carotenoids: Localisation and Function," In: D. R. Ort and C. F. Yocum, Eds., *Oxygenic Photosynthesis*: *The light reactions*, *Kluwer Academic Publishers*, Kluwer Academic Publishers, Dordrecht, 1996, pp. 539-563.

[26] V. Gavriušinas, J. Vaitkus and A. Vaitkuviené, "Methodology of Medical Diagnostics of Human Tissues by Fluorescence," *Lithuanian Journal of Physics*, Vol. 40, 2000, p. 232.

New Journal of Glass and Ceramics, **2011, 1, 13-19**
doi:10.4236/njgc.2011.11003 Published Online April 2011 (http://www.SciRP.org/journal/njgc)

Optimizing the Glass Fiber Cutting Process Using the Taguchi Methods and Grey Relational Analysis

Chao-Lieh Yang

Department of Industrial Engineering and Management Information, Huafan University, New Taipei City, Chinese Taipei.
Email: ygcl@ms38.hinet.net

Received March 10th, 2011; revised March 21st, 2011; accepted April 6th, 2011.

ABSTRACT

This paper mainly describes a new approach to optimizing of the cutting glass fiber with multiple performance characteristics, based on reliability analysis, Taguchi and Grey methods. During the cutting process, the speed, the volume and the cutting load are optimized cutting parameters when the performance characteristics, which include Weibull modulus and blade wear, are taken into consideration. In this paper, optimization with multiple performance characteristics is found to be the highest cutting speed and the smallest cutting volume, and the medium cutting load. An analysis of the variance of the blade wear indicates that the cutting speed (47.21%), *the cutting volume* (14.62%) *and the cutting load* (12.20%) *are the most significant parameters in the cutting process of glass fibers. In summary, the most optimal cutting parameter should be* $A3B1C2$. *The results of experiments have shown that the multiple performance characteristics of cutting glass fiber are improved effectively through this approach.*

Keywords**:** *Blade Wear*, *Cutting*, *Glass Fiber*, *Grey Relational Analysis*, *Optimizing*, *Taguchi Methods*

1. Introduction

Composite materials are playing an important role in a wide range of fields and replacing many traditional engineering materials. Glass fiber reinforced composite materials are a class of materials used in various products including aerospace, automobile, sporting goods, marine bodies, plastic pipes, storage containers, etc. An *et al.* [1] glass fiber reinforced plastic (GFRP) is characterized by high strength and rigidity coupled with low weight and, in many respects, is superior to metals. However, for the practical cutting of glass fiber, optimal cutting parameters should be taken into consideration to achieve less blade wear, good cutting quality, etc. In order to achieve this objective, how to control the blade wear correctly is decisive.

During glass fiber cutting, the reduction of blade wear is a critical aspect. Long glass fibers were found to affect cutting quality significantly. Lau *et al.* [2] showed that the wear characteristics of blades were highly influenced by the geometry and thickness of the blade. Casto *et al.* [3] discussed the lifetime according to different criteria, determined by using a profilometer and image processing, where the worn zone was observed using a scanning electron microscope (SEM). A Weibull distribution has been applied to a variety of cutting processes. Yang *et al.* [4] concluded that the effect of the cutting conditions, the cutting speed, the feed rate, and the depth of cut on the tool life and the cumulative probability of chipping could be presented as a Weibull distribution with three parameters. Lin [5] has observed that the cutting tool life can be represented for the cases studied by the statistical normal distribution. Moreover, Klim *et al.* [6] conducted a two-parameter study on the effect of feed variation on the tool wear and tool life, and found that this followed a Weibull distribution.

The Taguchi method [7] has produced a unique and powerful quality improvement discipline that differs from the traditional process. Since the product and process design have a great impact on the life cycle, the cost, and the quality of a component, the Taguchi design of experiment (DOE) approach provides a design engineer with a systematic method for determining the optimum design parameters to obtain the best performance at the lowest cost. Therefore, the Taguchi methods have become a widely acceptable methodology for improving productivity. However, the original Taguchi methods were designed to optimize a single performance characteristic. It is not the kind of condition that engineers deal with nowaday complex manufacturing process. Therefore, optimization of multiple performance characteristics is still interesting to researchers to do further study. Kang and Hadfield [8] designed a novel eccentric lapping machine, and in a systematic use of the Taguchi methods, they investigated the optimization of different lapping parameters. Lin [9] obtained optimal parameters using the Taguchi methods and analysis of the Weibull modulus through reliability engineering for the polishing of ceramic gauge blocks.

The Grey system theory proposed by Huang and Liao [10] has been proven to be useful for dealing with poor, incomplete, and unsure information. Chang *et al.* [11] presented a fast and effective methodology of Grey relational analysis for the optimization of the injection molding process parameters of short glass fiber reinforced polycarbonate composites. Lin and Lin [12] found the Grey relational analysis can be used to solve the electrical discharge machining (EDM) process with the multiple performance characteristics. The Grey relational analysis based on the Grey system theory by Deng [13] can be used to solve complicated inter-relationships among the multiple performance characteristics effectively.

To optimize several responses or quality characteristics simultaneously, many researchers have tried to combine the Taguchi methods with other methods [14,15]. Through the Grey relational analysis, a Grey relational grade is obtained to evaluate the multiple performance characteristics. As a result, optimization of the complicated multiple performance characteristics can be converted into optimization of a single Grey relational grade. Lin [14] has shown optimal cutting parameters can then be determined by the Taguchi methods using the Grey relational grade as the performance index. The cutting parameters, the tool life, the cutting force, and the surface roughness are important characteristics in turning. Lin *et al.* [15] used reliability analysis, the Taguchi and the Grey methods in this paper. The speed and the load are optimized polishing parameters when the performance characteristics, which include Weibull modulus and the removal rate, are taken into consideration.

In this paper, the reliability of the cutting process for glass fiber materials has been evaluated quantitatively in terms of a three-parameter Weibull distribution [4]. The effect of the cutting parameters, i.e. the cutting speed, the cutting volume, and the cutting load, on the blade wear, as determined by long glass fiber that would exceed a value of 1%, to meet the requirement of the customer acceptance standard TP-700 of the Owens Corning Company, was investigated. When using the Taguchi methods of parameter design, the experimental details were used for optimizing the single performance characteristics. Optimization of multiple performance characteristics with the Grey relational analysis was also considered in this paper. The methodology used in the experiments was the same as that used by Lin [9], and was as the following:

1) Perform a Taguchi-based experiment.
2) Measure the material wear from 12 cuts by a cutter blade.
3) Calculate the Weibull modulus and the mean value of the wear.
4) Calculate the signal-to-noise (*S*/*N*) ratio.
5) Collect the data while preprocessing both the mean value of the wear and the Weibull modulus.
6) Perform an analysis of variance (ANOVA) using the Grey relational analysis.
7) Carry out the confirmation runs.

2. Reliability Analysis

The reliability, determined from a three-parameter Weibull distribution, was expressed by Shigley *et al.* [16] as:

$$R = \exp-\left(\left(x-x_0\right)/\left(s-x_0\right)\right)^b \quad x \geq x_0 \tag{1}$$

In it:

x is the thin-edge blade wear (μm);

x_0 is the guaranteed value of y ($x_0 \geq 0$);

s is a characteristic or scale value ($s \geq x_0$);

b is the Weibull modulus ($b \geq 0$).

The Weibull modulus is the most important parameter in a Weibull distribution. The increases of reliability depend on the increase of the Weibull modulus. The probability of a failure, $F = 1 - R$, can be calculated as indicated by Shaw [17] according to:

$$F = \left(g-0.3\right)/\left(h+0.4\right) \tag{2}$$

In which:

g is the g^{th} sample as the blade wear values are ranked in order;

h is the total number of samples.

The detail for the relationship between the reliability and the wear rate has been derived by Yang *et al.* [4]. So, the guaranteed value x_0 can be written as

$$x_0 = x_2 - \frac{\left(x_3-x_2\right)\left(x_2-x_1\right)}{\left(x_3-2x_2+x_1\right)} \tag{3}$$

The characteristic parameter s can be written as

$$s = inv\ln\left(x-x_0\right)+x_0 \tag{4}$$

The Weibull modulus b can be written as

$$b = \Delta Y/\Delta x \tag{5}$$

3. Experiments

The identified parameters that affect the characteristics of turned parts are the cutting blade parameters (blade geometry and blade material), the workpiece-related parameters (long fiber), the cutting parameters (speed, load, and volume), and the environmental parameters (dry cutting and wet cutting). The ranges of the selected cutting process parameters (cutting speed V = 1.9 - 5.7 m/s, load F = 13 - 27 kgf/cm^2, and volume150 - 250 piece) are ascertained by conducting preliminary experiments. The details of the work material, the cutting machine, the cutting blade, and the cutting conditions are as the following:

The work material: E-glass fiber, 9 µm × 66 (g / 1000 m).

The cutting machine: Parallel blade-cutting machine (Finn and Fram, USA) with a 0.75 HP spindle power.

The cutting blade: Lutz cutter (Lutz, Germany) made of high-carbon steel disposable blades

The cutting condition: Dry

The wear measure: Examined by using a SEM to measure blade wear.

Glass fiber that were 9 µm in diameter and 66 (g / 1000 m) in weight and machined on a cutting machine with a carbon steel blade. The blade wear were measured by a SEM while each specimen was cut. The cutting blade samples were examined by a SEM to measure blade wear values at three points, and these were averaged to obtain an average blade wear value. Each cutting test of a blade wear was performed until the long glass fiber weight exceeded a value of 1%, as specified in the customer acceptance standard TP-700 of the Owens Corning Company.

4. The Single Performance Characteristic

4.1. The Taguchi Methods

An orthogonal array gives a more reliable estimate of the factor effects with fewer tests compared to traditional methods. In this paper, based on the experiments designed by Kang and Hadfield [8], three levels of cutting parameters were selected and the three cutting parameters were used as control parameters, and each parameter was designed to have three levels, as shown in **Table 1**. Three major control factors (cutting speed, load, and volume) were selected to conduct the tests. All three factors are multilevel variables and their outcome effects have nonlinear relationships; hence, we used three-level tests for each factor. The number of degrees of freedom was calculated from the number of parameters identified and their number of levels of variation. Using the full factorial design (3 × 3 × 3 × 3) reduced a total of 81 sets of experiments down to 9, thereby decreasing the cost, the time, and the effort. 9 the array along with the factors assigned to the columns was presented in **Table 2**, which consists of nine experiments corresponding to the nine rows and four columns. In this matrix, the chosen three parameters, the cutting speed, the cutting volume and the cutting load are assigned to the second, the third and the fifth columns. The fourth column was not assigned and used as an error term e. The nine experiments of the L9 array were carried out without the interaction effect.

4.2. Analysis of *S*/*N* ratio for the Smaller-the-Better Parameter

The Taguchi methods use the *S*/*N* ratio to analyze the average value of the test run data to derive values for evaluating the characteristic cutting parameters. This is because the *S*/*N* ratio represents both the average and the variation in quality characteristics. The units of the *S*/*N* ratio are decimals. The Taguchi parameter design is used to determine the optimum conditions of the engineering parameters (the controllable parameters), and also to minimize any variation in the noise (the uncontrollable parameters). The *S*/*N* ratio provides a measure of the robustness. To find the optimal cutting conditions, the blade wear should be of lower order; hence, the *S*/*N* for "the smaller the better" type of response is used:

$$S/N_{STB} = -10\log\left[1/n\sum y_i^2\right] \quad (6)$$

Table 1. Cutting parameters and levels.

Symbol	Parameter	Unit	Level 1	Level 2	Level 3
A	Cutting speed	m/s	1.9	3.8	5.7
B	Cutting volume	piece	150	200	250
C	Cutting load	Kgf/cm^2	27	20	13

Table 2. The L9 (3^4) orthogonal array used in Taguchi methods.

Group	A	B	e	C
1	1	1	1	1
2	1	2	2	2
3	1	3	3	3
4	2	1	2	3
5	2	2	3	1
6	2	3	1	2
7	3	1	3	2
8	3	2	1	3
9	3	3	2	1

where y_i is the mean value of the wear or Weibull modulus at the i^{th} test and n is the number of trials. S/N_{STB} is the smaller-the-better S/N ratio.

To understand the blade wear during cutting, an experiment using S55C high-carbon steel blades to cut the glass fiber was carried out as shown in the schematic diagram in **Figure 1**. In a single experiment, 12 cutting blades were used to cut simultaneously. **Table 3** shows the mean value of the wear and the corresponding *S/N* ratio calculated by using Equation (6). **Table 4** shows the Weibull modulus and the corresponding *S/N* ratio calculated by using Equation (6).

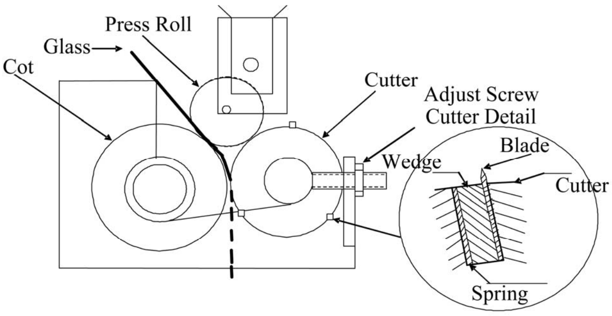

Figure 1. Schematic of cutting machine.

Table 3. Experimental results for the mean value of the wear and the S/N ratio.

Group	Mean value of wear (μm)	*S/N* ratio (dB)
1	49.29	–33.93
2	40.03	–32.24
3	39.58	–32.04
4	63.05	36.05
5	59.01	–35.46
6	55.21	–34.93
7	39.78	–32.06
8	64.39	–36.22
9	48.17	–33.79

Table 4. Experimental results for the Weibull modulus and the *S/N* ratio.

Group	Weibull modulus	*S/N* ratio (dB)
1	2.07	–6.32
2	8.65	–18.74
3	3.69	–11.34
4	6.75	–16.59
5	3.34	–10.47
6	6.04	–15.62
7	1.85	–5.34
8	4.27	–12.61
9	1.89	–5.53

5. Multiple Performance Characteristics

5.1. Grey Relational Analysis

In the Grey relational analysis, a data preprocessing is first performed in order to normalize the raw data, and a linear normalization of the experimental results for the mean value of the wear and the Weibull modulus is performed in the range between zero and one, which is also called the Grey relational generating [13,18].

For the blade wear and weibull modulus, which are "the smaller the better", the normalized *S/N* ratio z_{ij} for the i^{th} performance characteristic in the j^{th} can be expressed as

$$z_{ij} = \frac{\max y_{ij} - y_{ij}}{\max\limits_{j} y_{ij} - \min\limits_{j} y_{ij}} \tag{7}$$

y_{ij} for the i^{th} experimental results in the j^{th} experiment.

Next, the Grey relational coefficient is calculated to express the relationship between the ideal (best) and the actual normalized *S/N* ratio. The Grey relational coefficient α_{ij} for the ith performance characteristic in the j^{th} experiment can be expressed as

$$\alpha_{ij} = \frac{\min\limits_{i}\min\limits_{j}\left|z_i^0 - z_{ij}\right| + \beta \max\limits_{i}\max\limits_{j}\left|z_i^0 - z_{ij}\right|}{\left|z_i^0 - z_{ij}\right| + \beta \max\limits_{i}\max\limits_{j}\left|z_i^0 - z_{ij}\right|} \tag{8}$$

where z_i^0 is the ideal normalized *S/N* ratio for the i^{th} performance characteristics and β distinguishing coefficient which is setting as 0.5 in this article.

Then, the Grey relational grade is computed by averaging the Grey relational coefficient corresponding to each performance characteristic. The overall evaluation of the multiple performance characteristics is based on the Grey relational grade, that is

$$\gamma_j = \frac{1}{k}\sum_{i=1}^{k} \alpha_{ij} \tag{9}$$

In it:

γ_j is the Grey relational grade for the j^{th} experiment;

k is the number of performance characteristics.

Table 5 shows the dada calculated by using Equation (7), the normalized results for the mean value of the blade wear and the Weibull modulus. Basically, the larger normalized results correspond to the better performance and the best normalized results should be equal to one. The grey relational coefficient results for the experimental layout are shown in **Table 6**.

Using the experimental combinations of **Table 2**, **Table 7** shows the Grey relational grade for each experiment. The larger Grey relational grade indicates that the corresponding experimental result is closer to the ideally normalized value. Group 7 has the best multiple performance characteristics among the nine experiments because it has the highest Grey relational grade shown in **Table 7**. Since the experimental design is orthogonal, it is then possible to separate out the effect of each cutting parameter in different levels.

Figure 2 shows the Grey relational grade graph, where the dashed line in this figure is the value of the total mean of the Grey relational grade. Basically, the larger the Grey relational grade is, the better the multiple performance characteristics are. A3B1C2 is the optimal level of cutting parameters with the multiple performance characteristics.

Table 5. Data preprocessing of experimental result for each performance characteristic.

Group	Mean value of wear (μm)	Weibull modulus
1	0.4504	0.0729
2	0.0466	1.0000
3	0.0000	0.4476
4	0.9583	0.8392
5	0.8192	0.3830
6	0.6921	0.7671
7	0.0032	0.0000
8	1.0000	0.5423
9	0.4183	0.0139

Table 6. Grey relational coefficient of each performance characteristic.

Group	Mean value of wear (μm)	Weibull modulus
1	0.5261	0.8728
2	0.9147	0.3333
3	1.0000	0.5276
4	0.3429	0.3734
5	0.3790	0.5662
6	0.4194	0.3946
7	0.9936	1.0000
8	0.3333	0.4797
9	0.5445	0.9730

Table 7. Grey relational grade for each experiment.

Group	Grey relational grade	Order
1	0.6994	4
2	0.6240	5
3	0.7638	2
4	0.3581	9
5	0.4726	6
6	0.4070	7
7	0.9968	1
8	0.4065	8
9	0.7588	3

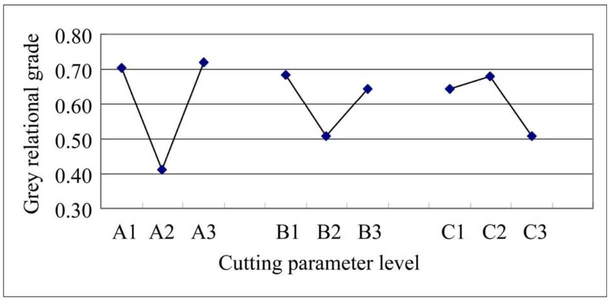

Figure 2. Grey relational grade graph.

5.2. Analysis of Variance

The ANOVA scheme was used to study the significance of the parameters affecting the quality characteristics of the interest. The scheme subdivides the total variation in the data into useful and meaningful components of variation. The total variation contribution is shown in **Table 8**. The ANOVA results in Table 8 clearly identify that the cutting speed and the volume severely affected the blade wear by 47.21% and 14.62%, respectively, while the load only affected the blade wear by 12.20%.

5.3. Confirmation Tests

A confirmation experiment is the final step in the design of experiment process. Once the optimum level of the design parameters is set, the final step can predict and verify the quality characteristic using the optimum level η_{opt} of the design parameters, which can also be estimated by using the equation

$$\eta_{opt} = \overline{\eta} + \sum_{j=1}^{0} \left(\eta_i - \overline{\eta} \right) \quad (10)$$

In which:

$\overline{\eta}$ is the mean of the *S*/*N* ratio;

η_j is the *S*/*N* ratio at the optimum level;

o is the number of main design parameters that affects the optimum level of the cutting parameters.

From Equation (10), the estimated optimum design parameters can be obtained by using the optimum cutting parameters.

A pareto chart generated based on the contribution ratio is presented in **Figure 3**. This chart shows the importance of the significant parameters. **Table 9** shows a comparison among the initial, predicted, and confirmation experimental values of the wear, respectively, using the optimum cutting parameters. **Table 9** shows the results of the confirmation experiment for the mean value of the wear. The results of the confirmation experiment of the predicted optimal conditions A3B1C2, which was better than the initial trial. As shown in **Table 9**, the blade wear decreases from 64.73 to 39.43, when the

Table 8. Results of analysis of variance for multiple performance characteristic.

Symbol	Cutting parameter	Sum of square	Degree of freedom	Contribution (%)
A	Cutting speed	0.18	2	47.21
B	Cutting volume	0.06	2	14.62
C	Cutting load	0.05	2	12.20
Error		0.09	2	25.97
Total		0.37	8	100.00

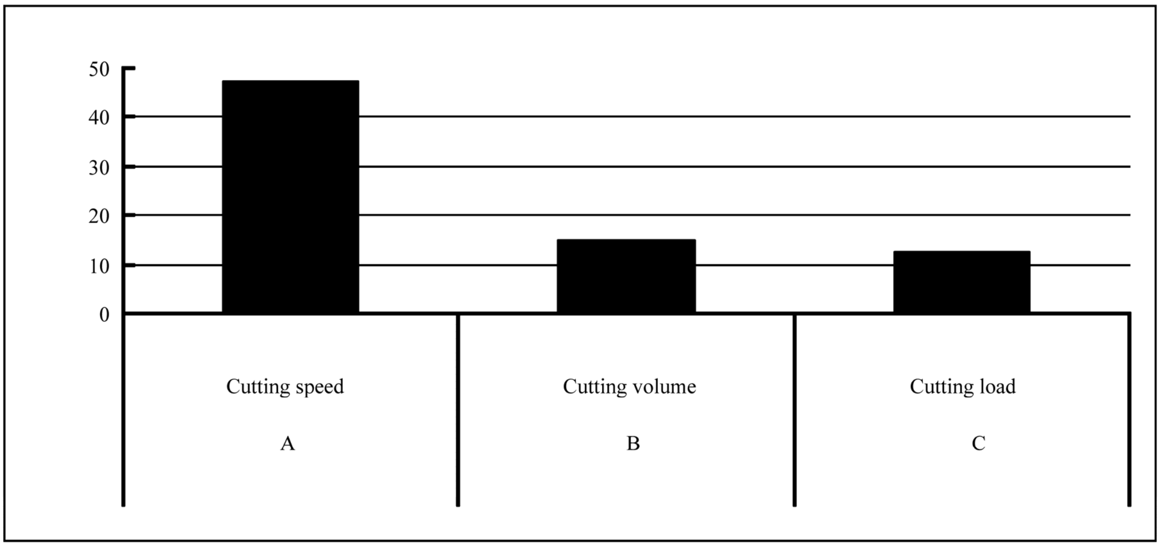

Figure 3. Pareto chart.

Table 9. Results of the confirmation experiment.

Cutting parameter	Initial	Predicted	Confirmation experiment
Level	A2B2C2	A3B1C2	A3B1C2
Wear (μm)	64.73	-	39.43
Weibull modulus	1.90	-	1.85
Grey relational grade	0.4498	0.9332	0.9968
Improvement of grey relational grade	-	-	0.5470
Improvement in wear (%)	-	-	64.16

Weibull modulus is decreased from 1.9 to 1.85. In summary, the most optimal cutting parameter should be A3B1C2, because the improvement is the greatest by using this parameter, and it is obvious that the optimum level of the cutting parameters in the cutting process is greatly improved.

Conducting a verification experiment is a crucial and the last step of the robust design procedure. Its aim is to verify the optimum conditions identified by the matrix tests and it estimates how close the predictions are to actual conditions. Hence, a confirmation test was conducted with the optimum parameters, and came out in good result.

6. Conclusions

This paper has carried out the optimization in the cutting of glass fiber. The following conclusions are obtained from analyzing the above stated experimental results:

1) The multiple parameters for multiple performance characteristics are found to be the higest speed, the smaller cutting volume and the medium load.

2) To study further within the experimental range used, we found that the most significant cutting parameter for multiple performance characteristics are the cutting speed, which accounts for 47.21% of the total effect, followed by the cutting volume (14.62%), and the cutting load, which accounts for only 12.20% of the total effect.

3) In summary, the most optimal cutting parameter is A3B1C2.

4) In the cutting glass fiber, using reliability analysis with Grey-based Taguchi methods is a good way to improve the multiple performance characteristics.

REFERENCES

[1] S. O. An, E. S. Lee and S. L. Noh, "A Study on the Cutting Characteristics of Glass Fiber Reinforced Plastics with Respect to Tool Materials and Geometries," *Journal of Materials Processing Technology*, Vol. 68, No. 1, 1997, pp. 60-67. doi:10.1016/S0924-0136(96)02534-4

[2] K. H. Lau, D. Mei, C. F. Yeung and H. C. Man, "Wear Characteristics and Mechanisms of a Thin Edge Cutting Blade, "*Journal of Materials Processing Technology*, Vol. 102, No. 1-3, 2000, pp. 203-207. doi:10.1016/S0924-0136(99)00410-0

[3] S. L. Casto, E. L. Valvo, E. Lucchini, S. Maschio and V. F. Ruisi, "Wear Rates and Wear Mechanisms of Alumina-Based Tools Cutting Steel at a Low Cutting Speed," *Wear*, Vol. 208, No. 1-2, 1997, pp. 67-72. doi:10.1016/S0043-1648(96)07376-0

[4] C. L. Yang, S. H. Sheu and K.T. Yu, "The Reliability Analysis of a Thin-Edge Blade Wear in the Glass Fiber Cutting Process," *Journal of Materials Processing Technology*, Vol. 209, No. 4, 2009, pp. 1789-1795. doi:10.1016/j.jmatprotec.2008.04.028

[5] W. S. Lin, "The Reliability Analysis of Cutting Tools in the HSM Processes," *Archives of Materials Science and Engineering*, Vol. 30, No. 2, 2008, pp. 97-100.

[6] Z. Klim, E. Ennajimi, M. Balazinski and C. Fortin, "Cutting Tool Reliability Analysis for Variable Feed Milling of 17-4PH Stainless Steel," *Wear*, Vol. 195, No. 1-2, 1996, pp. 206-213. doi:10.1016/0043-1648(95)06863-5

[7] P. J. Ross, "Taguchi Techniques for Quality Engineering," McGraw-Hill Book Company Press, New York, 1996.

[8] J. Kang and M. Hadfield, "Parameter Optimization by Taguchi Methods for Finishing Advanced Ceramic Balls Using a Novel Eccentric Lapping Machine," *Proceedings of the Institution of Mechanical Engineers*, *Part B*: *Journal of Engineering Manufacture*, Vol. 215, No. 1, 2001, pp. 69-78. doi:10.1243/0954405011515145

[9] T. R. Lin, "The Use of Reliability in the Taguchi Method for the Optimization of the Polishing Ceramic Gauge Block," *The International Journal of Advanced Manufacturing Technology*, Vol. 22, No. 3-4, 2003, pp. 237-242. doi:10.1007/s00170-002-1465-1

[10] J. T. Huang and Y. S. Liao, "Optimization of Machining Parameters of Wire-EDM Based on Grey Relational and Statistical Analyses," *International Journal of Production Research*, Vol. 41, No. 8, 2003, pp. 1707-1720. doi:10.1080/1352816031000074973

[11] S. H. Chang, J. R. Hwang and J. L. Doong, "Optimization of the Injection Molding Process of Short Glass Fiber Reinforced Polycarbonate Composites Using Grey Relational Analysis," *Journal of Materials Processing Technology*, Vol. 97, No. 1-3, 2000, pp. 186-193. doi:10.1016/S0924-0136(99)00375-1

[12] J. L. Lin and C. L. Lin, "The Use of the Orthogonal Array with Grey Relational Analysis to Optimize the Electrical Discharge Machining Process with Multiple Performance Characteristics," *International Journal of Machine Tools and Manufacture*, Vol. 42, No. 2, 2002, pp. 237-244. doi:10.1016/S0890-6955(01)00107-9

[13] J. L. Deng, "Introduction to Grey System Theory," *Journal of Grey System*, Vol. 1, No. 1, 1989, pp.1-24.

[14] C. L. Lin, "Use of the Taguchi Method and Grey Relational Analysis to Optimize Turning Operations with Multiple Performance Characteristics," *Materials and Manufacturing Processes*, Vol. 19, No. 2, 2004, pp. 209-220. doi:10.1081/AMP-120029852

[15] T. R. Lin, H. C. Chiu and M. F. Huang, "Optimizing Removal Rate and Reliability of Polishing of Ceramic Blocks Using a Combination of Taguchi and Grey Method," Institute of Materials Minerals an Mining, August 2004.

[16] J. E. Shigley, C. R. Mischke and R. G. Budynas, "Mechanical Engineering Design," 7th Edition, McGraw-Hill Press, New York, 2003.

[17] M. C. Shaw, "Metal Cutting Principles," Oxford Science Press, New York, 2004.

[18] K. L. Wen, Y. W. Huang, W. C. Chung, T. C. Chung, M. L. You and C. J. Lai, "Method and Application of Grey Model," Gau-Lih Press, Taipei, 2003.

